Progress in Natural Science: Materials International 36 (2026) 110–118

HOSTED BY

Contents lists available at ScienceDirect

Progress in Natural Science: Materials International

journal homepage: www.elsevier.com/locate/pnsmi

Significantly improving the bending formability of AZ31 Mg alloy by pre-introducing {10 $\bar{1}$ 2} tensile twins

Longhui Sun[a,1], Hongchen Jing[a,1], Hua Zhang[a,*], Liying Sun[a], Lifei Wang[b], Liwei Lu[c], Kwang Seon Shin[a,d], T.B. Duishenaliev[e]

[a] Shandong Key Laboratory of Advanced Structural Materials Genome Engineering, Yantai University, Yantai, 264005, China
[b] Department of Materials Science and Engineering, Taiyuan University of Technology, Taiyuan, 030024, China
[c] Hunan Provincial Key Laboratory of High Efficiency and Precision Machining of Difficult-to-Cut Material, Hunan University of Science and Technology, Xiangtan, 411201, China
[d] Research Institute of Advanced Materials, Seoul National University, Seoul, 08826, South Korea
[e] Kyrgyz State Technical University Named After Iskhak Razzakov, Bishkek, 720044, Kyrgyzstan

ARTICLE INFO

Keywords:
Mg alloy
Pre-compression
Tension-compression asymmetry
Bending behavior
{10 1^{-} 2} tensile twin

ABSTRACT

{10 $\bar{1}$ 2} tensile twins were introduced by pre-compressing the rolled AZ31 Mg alloy sheet along the transverse direction (TD) with a strain of 3 %, aiming to investigate the effect of pre-existing twins on its bending deformation behavior. For the AZ31 Mg alloy, the pre-existing {10 $\bar{1}$ 2} tensile twins significantly improved the mechanical properties, the tension-compression yield asymmetry coefficient (0.57 vs. 0.35), and the bending property (bend angle: 97° vs. 65°). The pre-existing {10 $\bar{1}$ 2} twins led to the deflection of the c-axis of the grains, thus modifying the strong (0001) basal texture, which improved the tension-compression yield asymmetry, making the strain distribution during the bending process in each region of the specimen more uniform. The basal slip caused by grain deflection on the rolling direction (RD)-normal direction (ND) plane increased the thickness-direction strain of the specimen during the bending deformation process. Moreover, the introduction of a large number of twin lamellae effectively subdivided and refined the grains, enhancing the plastic deformation ability of the specimen. In summary, these factors led to a significant improvement in the bending formability of the AZ31 Mg alloy.

1. Introduction

Mg alloy, recognized as one of the lightest metal structural materials, is widely applied in the fields of new energy vehicles and aerospace equipment manufacturing and biodegradable implants [1–3]. However, Mg alloy has a hexagonal close-packed (HCP) crystal structure, which leads to a limited number of slip systems during plastic deformation. Furthermore, at room temperature, non-basal slip typically requires extremely high critical resolved shear stress (CRSS) to be activated [4,5]. This results in poor room temperature plasticity and inadequate formability, such as bending performance, in Mg alloy, significantly restricting their large-scale application in industrial production. In Mg alloy, the critical resolved shear stress required for {10 $\bar{1}$ 2} tensile twinning is relatively low, only slightly higher than that for basal slip, which makes it easily activated at room temperature [6,7]. In view of this, introducing {10 $\bar{1}$ 2} tensile twins through pre-deformation to regulate the microstructure of Mg alloy is regarded as an effective strategy for improving its properties [8–12].

Li et al. [8] found that when the AZ31 Mg alloy was subjected to 3 % compressive deformation, the average grain size significantly decreased from 37.9 μm to 18.9 μm due to the formation of a large number of layered twin bands, and a new crystallographic texture with the c-axis parallel to the transverse direction (TD) was generated, which weakened the initial (0001) basal texture oriented along the normal direction (ND). Chen et al. [9] suggested that the yield strength of extruded AZ31 Mg alloy was improved by pre-compression and heat treatment, and this improvement was attributed to the twins introduced by pre-compression, which provided more nucleation sites for the recrystallization process, thereby refining the grain structure. Huang et al. [10] investigated the effect of {10 $\bar{1}$ 2} twins introduced by

* Corresponding author.
E-mail address: zhanghua@ytu.edu.cn (H. Zhang).
[1] L.H. Sun and H.C. Jing contributed to the work equally.

https://doi.org/10.1016/j.pnsc.2025.12.002
Received 22 September 2025; Received in revised form 5 December 2025; Accepted 8 December 2025
Available online 3 January 2026

pre-compression on the low-cycle fatigue performance and cyclic deformation behavior of rolled AZ31 Mg alloy, and the results showed that at low-stress amplitude, the fatigue life of the pre-compressed samples was significantly longer than that of the as-rolled samples, as the twinning-detwinning behavior induced by the {10 $\bar{1}$ 2} twins introduced by pre-compression changed the deformation mechanism. Zhang et al. [11] found that pre-twinning significantly increased the compressive yield strength of AZ31 Mg alloy at temperatures from room temperature to 200 °C, but the effect of pre-existing twins on yield strength disappeared at 200 °C due to the occurrence of dynamic recrystallization. Park et al. [12] increased the Erichsen value of AZ31 Mg alloy from 3.1 mm in the initial state to 6.3 mm through 8 % pre-compression, and suggested that detwinning in the twinned regions and the activation of basal slip effectively accommodated the thickness strain, leading to the improvement of deep drawing performance. Lee et al. [13] studied texture tailoring and bendability improvement of rolled AZ31 alloy using {10 $\bar{1}$ 2} twinning, and attributed the improvement in the bending formability to the change in texture, the significant activation of twinning, and the enhancement of basal slip.

In summary, recent studies indicate that pre-introducing {10 $\bar{1}$ 2} tensile twins through pre-deformation have great potential to enhance the mechanical properties of AZ31 Mg alloy. Although some reports have focused on improving the bending formability of AZ31 Mg alloy through pre-introducing {10 $\bar{1}$ 2} tensile twins, the understanding of the reasons for this improvement is not comprehensive. In addition to the influence of pre-existing {10$\bar{1}$ 2} twins on the microstructure, research on their influence on tension-compression yield asymmetry and its consequent effect on the bending formability has never been thoroughly reported. Based on this, the purpose of this study is to explore the improvement of the bending formability of AZ31 magnesium alloy by pre-introducing {10 $\bar{1}$ 2} twins and to systematically investigate the reasons for its improvement.

2. Experimental procedure

This study utilized a 30 mm thick commercial hot-rolled AZ31 Mg alloy plate (chemical composition: Mg-3 wt.% Al-1 wt.% Zn). Rectangular block samples with dimensions of 55 mm (Rolling direction, RD), 35 mm (TD), and 30 mm (ND) were cut from the initial material. Subsequently, these rectangular block samples were pre-compressed along TD to a plastic strain of 3 % at room temperature to pre-introduce {10 $\bar{1}$ 2} tensile twins. Afterward, the pre-compressed block samples were annealed at 200 °C for 6 h to relieve dislocations and residual stress generated during the pre-compression process while retaining the twin structure.

Specimens were cut respectively from the initial as-received (AR) sample and the pre-compressed (PC) sample for tensile, compressive, and bending tests, where the tensile load, compressive load, and bending load were all parallel to the ND. The gauge dimensions of the tensile specimen were 3 mm (TD) × 1 mm (RD) × 30 mm (ND), the dimensions of the compression specimen were 5 mm (TD) × 5 mm (RD) × 10 mm (ND), and the dimensions of the bending specimen were 3.5 mm (ND) × 4.5 mm (TD) × 53 mm (RD). Room temperature tensile, compression, and bending experiments were conducted on a SANS-CMT5205 10 kN electronic universal testing machine, where the speeds for tensile and compression tests were 0.6 mm/min, and the bending indenter speed was 2 mm/min. The experiment was repeated three times for each state sample, and the average value was taken as the result.

Microstructure observation was performed using scanning electron microscopy (TESCAN VEGA) equipped with an EBSD probe (Oxford C-Nano). Samples for EBSD observation were prepared by mechanical grinding using 2000-grit SiC paper, followed by electropolishing for 45–80 s using ACII electrolyte at 15 V and −30 °C. EBSD was performed at 20 kV, 15 mm working distance, 70° tilt angle, and a 1 μm scan step size. The acquired EBSD data were analyzed using Aztec Crystal software.

3. Results

3.1. Initial microstructure

Fig. 1 shows the microstructure characteristics of the AR specimen. Fig. 1a displays that the microstructure of the AR specimen is composed of a few coarse grains and a large number of equiaxed grains, with no obvious deformed grain features observed. Fig. 1c shows that its average grain size is 33.57 μm. The (0001) pole figure in Fig. 1b shows that the texture is concentrated in the central area, indicating a strong preferred orientation of the grains, and no obvious preferred orientation distribution is found on the {10 $\bar{1}$ 0} prismatic planes. Fig. 1d shows that the proportion of high-angle grain boundaries (HAGBs, misorientation angle >15°) is 82.8 %, and the proportion of low-angle grain boundaries (LAGBs, misorientation angle ≤15°) is 17.2 %, indicating no obvious substructure within the material.

Fig. 2 shows the microstructure characteristics of the PC specimen. Because the direction of the pre-compression stress is perpendicular to the c-axis of the grain, the grain orientation is favorable for the activation of {10 $\bar{1}$ 2} tensile twinning [12], thus numerous {10 $\bar{1}$ 2} tensile twins appeared in the PC specimen (Fig. 2a and d), and the area fraction of {10 $\bar{1}$ 2} tensile twins are approximately 33.75 %. Moreover, the activation of {10$\bar{1}$ 2} twins led to the grain rotating by 86.3° towards the stress direction [14,15], so a TD-oriented twin texture was formed in the PC specimen, and there was no obvious preferred orientation on the {10 $\bar{1}$ 0} prismatic planes, as shown in Fig. 2b. Fig. 2c shows that the average grain size of the PC specimen is refined to 26.40 μm compared to that of the AR specimen, which can be attributed to the formation of a large number of twin lamellae [16,17]. Fig. 2d shows the misorientation distribution map in the PC specimen annealed at 200 °C for 6h, and the proportion of HAGBs reached 90.3 %, indicating no obvious substructure within the material, and the influence of distortion introduced by pre-compression can be ignored. In addition, a peak around 85° appeared in the misorientation distribution map, which corresponds to the formation of numerous new {10 $\bar{1}$ 2} tensile twin boundaries in the microstructure.

3.2. Tension-compression asymmetry

Fig. 3 shows the uniaxial tensile and compressive stress-strain curves of the AR and PC specimens along RD at room temperature. Table 1 summarizes the corresponding mechanical properties, such as yield strength, peak stress, plasticity index (elongation or compression ratio), and tension-compression asymmetry coefficient (compression yield strength/tension yield strength, CYS/TYS). As can be seen, the pre-existing {10 $\bar{1}$ 2} tensile twins significantly affect the uniaxial mechanical properties. The pre-existing {10$\bar{1}$ 2} tensile twins significantly increase the tension yield strength (191 MPa vs. 151 MPa) and compression yield strength (108 MPa vs. 53 MPa). The tension peak stress (305 MPa vs. 283 MPa), compression peak stress (302 MPa vs. 275 MPa), elongation (15.7 % vs. 12.8 %), and compression ratio (17.0 % vs. 15.1 %) also show corresponding increases. It is noteworthy that the pre-existing {10$\bar{1}$ 2} tensile twins improve the tension-compression asymmetry of the Mg alloy along RD, where the tension-compression yield asymmetry coefficient increased from 0.35 to 0.57. When an Mg alloy plate exhibits tension-compression yield asymmetry, its stress distribution during bending is no longer symmetric [18,19]. Significant tension-compression yield asymmetry, especially when the compression yield strength is much lower than the tensile yield strength, often limits the bending formability of materials [20,21]. Premature yielding on the compressive side can lead to local buckling or cracking during, thereby limiting the achievable bending angle without failure.

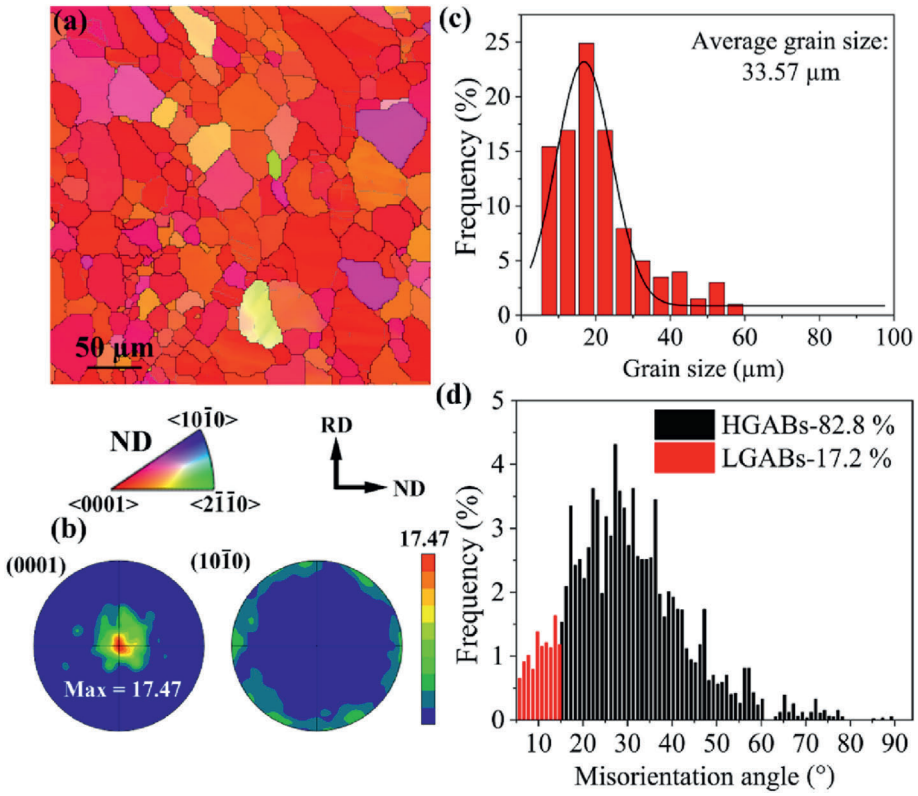

Fig. 1. Microstructure characteristics of the AR specimen: (a) inverse pole figure (IPF), (b) pole figures, (c) grain size distribution, and (d) misorientation distribution.

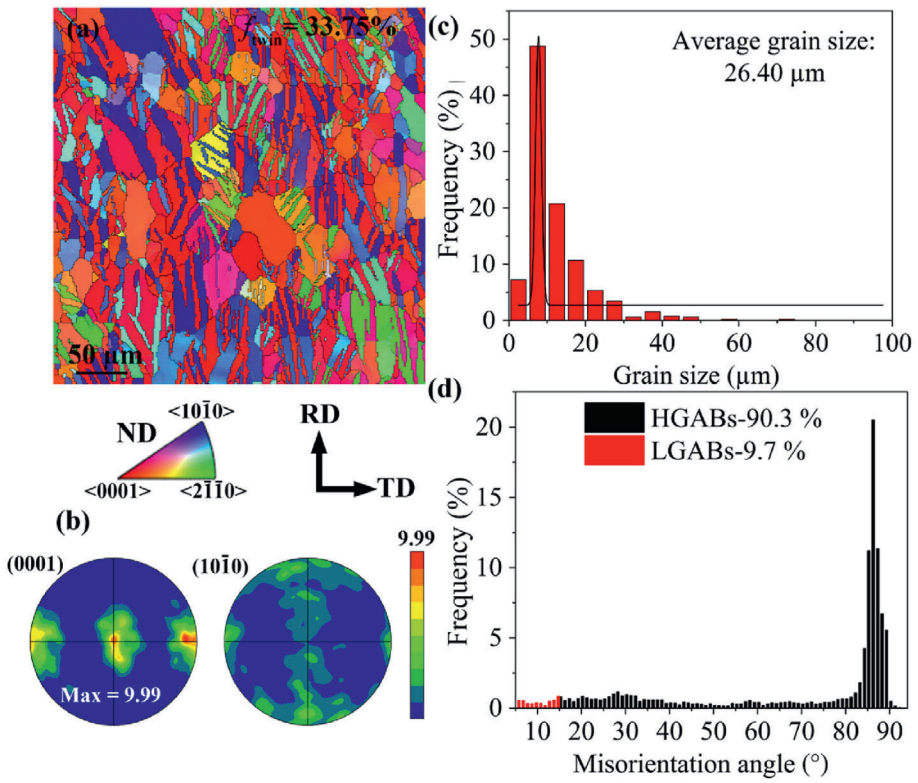

Fig. 2. Microstructure characteristics of the PC specimen: (a) IPF, (b) pole figures, (c) grain size distribution, and (d) misorientation distribution.

The improvement in the tension-compression asymmetry reduces the neutral axis shift and makes the stress distribution more uniform in the specimen during bending [22]. Meanwhile, as the stress concentration in the tensile zone on the outer side of the specimen during bending is

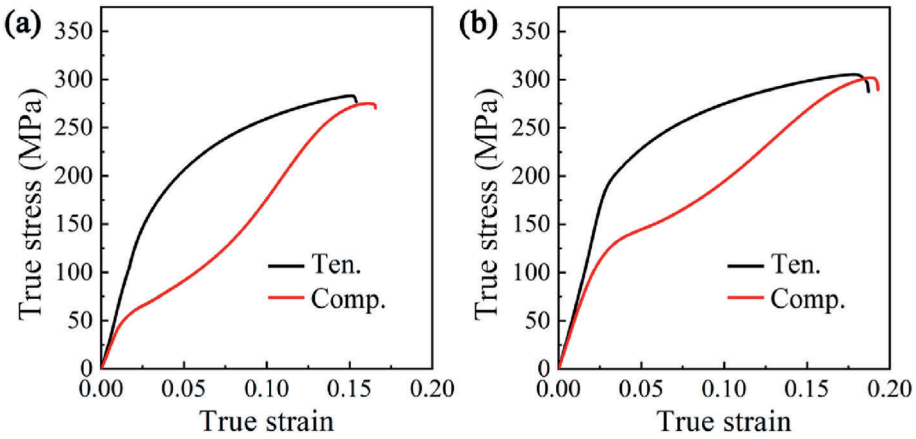

Fig. 3. Uniaxial tensile and compressive stress-strain curves along RD: (a) AR specimen, and (b) PC specimen.

Table 1
Uniaxial tension/compression mechanical properties of AR and PC specimens along the RD.

Specimen	Loading	Yield stress (MPa)	Peak stress (MPa)	Plasticity index (%)	Tension-compression asymmetry (CYS/TYS)
AR	Tension	151 ± 2	283 ± 2	12.8 ± 1	0.35
	Compression	53 ± 1	275 ± 4	15.1 ± 2	
PC	Tension	191 ± 3	305 ± 3	15.7 ± 2	0.57
	Compression	108 ± 2	302 ± 5	17.0 ± 3	

alleviated, it can withstand greater deformation without fracturing. Therefore, the improvement in tension-compression yield asymmetry is beneficial for the PC sample to be bent to a larger angle without cracking.

3.3. Improvement in bending formability

Fig. 4 shows the bending formability of the AR and PC specimens at room temperature. It can be found that, compared to the AR specimen, which has a bending angle of 65° and a bending press head displacement of 7.3 mm, the PC specimen achieves a bending angle of 97° and a bending press head displacement of 12.2 mm, indicating a significant improvement in bending formability. Furthermore, similar to the uniaxial tension/compression results, pre-existing {10 $\bar{1}$ 2} tensile twins also improve the bending yield strength and bending peak stress. Firstly, a large number of {10$\bar{1}$ 2} tensile twin lamellae introduced by pre-compression subdivide the grains. This leads to a reduction in grain size, thereby increasing the strength [20]. Secondly, a large number of {10 $\bar{1}$ 2} tensile twin lamellae can effectively hinder dislocation slip, thus increasing strength [23].

3.4. Microstructural evolution during bending

Fig. 5 displays the EBSD characteristics in different regions of the AR and PC specimens after bending deformation. It can be found that compared to the bent AR sample, the bent PC sample shows a larger area fraction of {10 $\bar{1}$ 2} tensile twins in different regions (inner region: 36.39 % vs. 21.05 %, middle region: 29.01 % vs. 7.50 %, and outer region: 21.13 % vs. 6.61 %). The twins in the bent AR specimen are mostly mutually parallel narrow lenticular twins, while in the bent PC specimen, there are not only mutually parallel narrow lenticular twins, but also intersecting twins, fragmented twins, and even coarse twins occupying entire grains. Furthermore, new twins generated during the bending process in the PC specimen interact with the pre-existing twins,

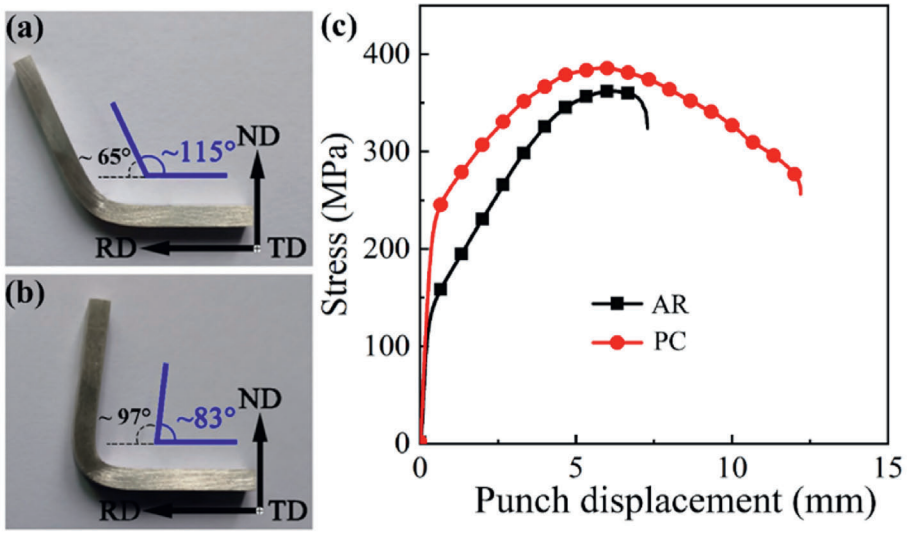

Fig. 4. Bending properties of the AR and PC specimens: (a) final bent AR specimen; (b) final bent PC specimen; (c) corresponding stress vs. punch displacement curves.

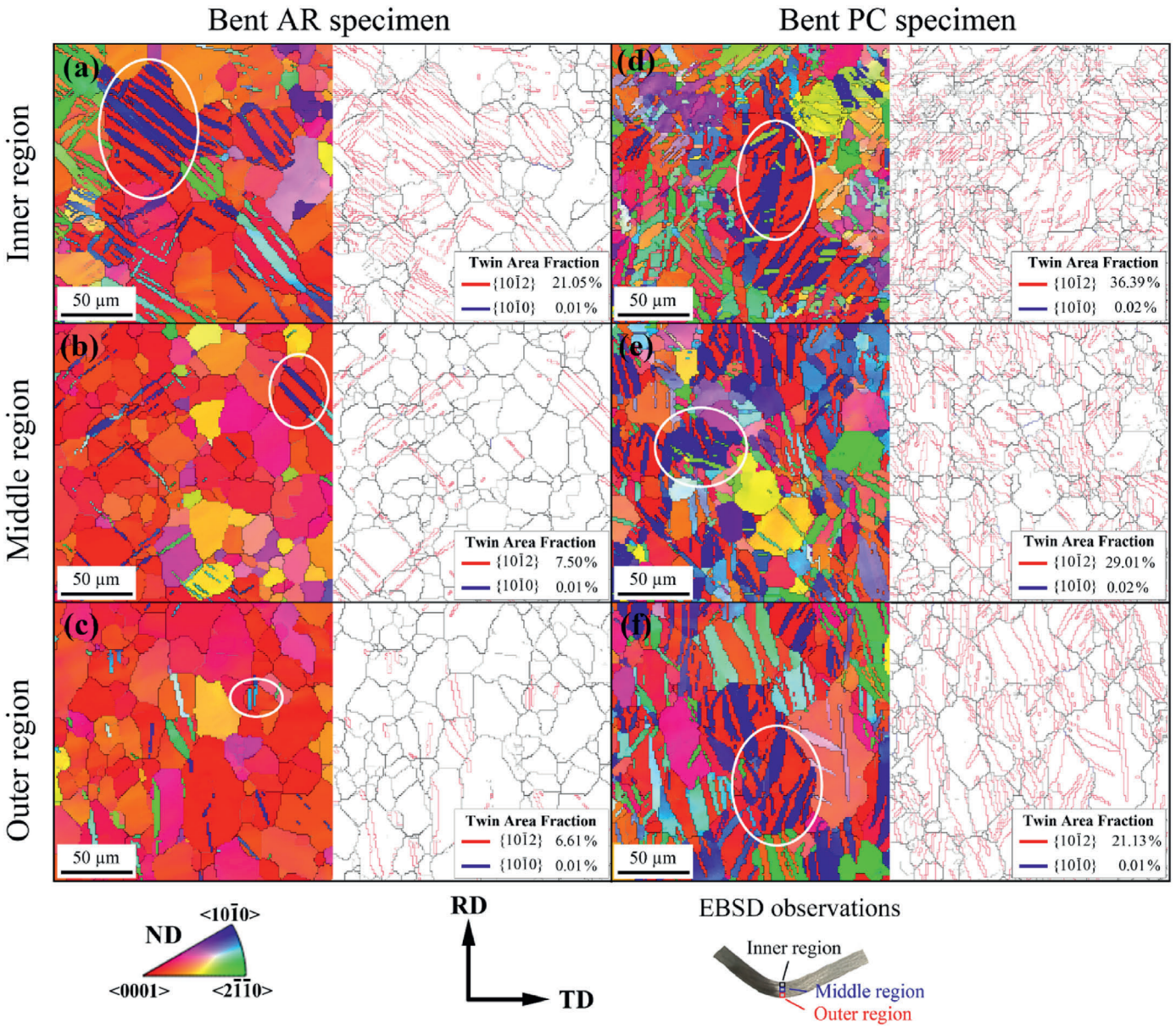

Fig. 5. EBSD characteristics in different regions of bent specimens: (a) (b) (c) bent AR specimen, and (d) (e) (f) bent PC specimen.

and their growth is restricted by the pre-existing twin boundaries. New twins in the PC specimen during the bending process tend to form within the pre-existing twins, which is mainly attributed to the pre-existing twin boundaries acting as interfaces between regions with different orientations, whose crystallographic discontinuity, high distortion, and high defect density are prone to cause stress concentration [24,25]. In addition, forming new twins within the pre-existing twins helps coordinate strain compatibility and lowers the nucleation energy barrier.

We distinguish the existing twins from the newly-formed twins primarily based on their morphology and spatial relationship. The pre-existing twins, introduced by pre-compression, are typically large, broad, and tend to be parallel within the grains. In contrast, the newly-formed twins generated during the bending process often exhibit distinct characteristics: they appear as intersecting twins cutting across pre-existing twins, or as fragmented/restricted twins nucleating and growing within the pre-existing twin lamellae.

In the bent AR specimen, the area fraction of {10 $\bar{1}$ 2} tensile twins gradually decrease from the inner region to the outer region, which is primarily due to the influence of the stress state during bending. During bending, the inner region of the bent specimen is under compression, and the compressive stress is perpendicular to the *c*-axis of the grain, which is favorable for the formation of {10 $\bar{1}$ 2} tensile twins with low CRSS [26,27]. The outer region of the bent specimen is under tension, and the tensile stress is perpendicular to the *c*-axis of the grain, which is unfavorable for the formation of {10 $\bar{1}$ 2} tensile twins. In the bent PC specimen, the compressive stress in the inner region is also favorable for {10$\bar{1}$ 2} twinning, and the high-stress level also drives pre-existing twin boundary migration and growth [28], with some twins even occupying entire grains, increasing the area fraction of {10 $\bar{1}$ 2} tensile twins from 31.02 % in the PC sample to 36.39 %. In the middle region of the bent PC specimen, the strain level is low, which is insufficient to drive new twin nucleation, thus resulting in little change in the twin area fraction (29.01 % vs. 31.02 %). In the outer region of the bent PC specimen, the tensile stress state is unfavorable for the formation of {10$\bar{1}$ 2} tensile twins and leads to detwinning [16,29,30], causing the area fraction of {10 $\bar{1}$ 2} tensile twins to decrease to 21.13 %.

Fig. 6 shows the local twinning features in the AR and PC specimens during the bending process. As can be seen from the (0001) pole figures,

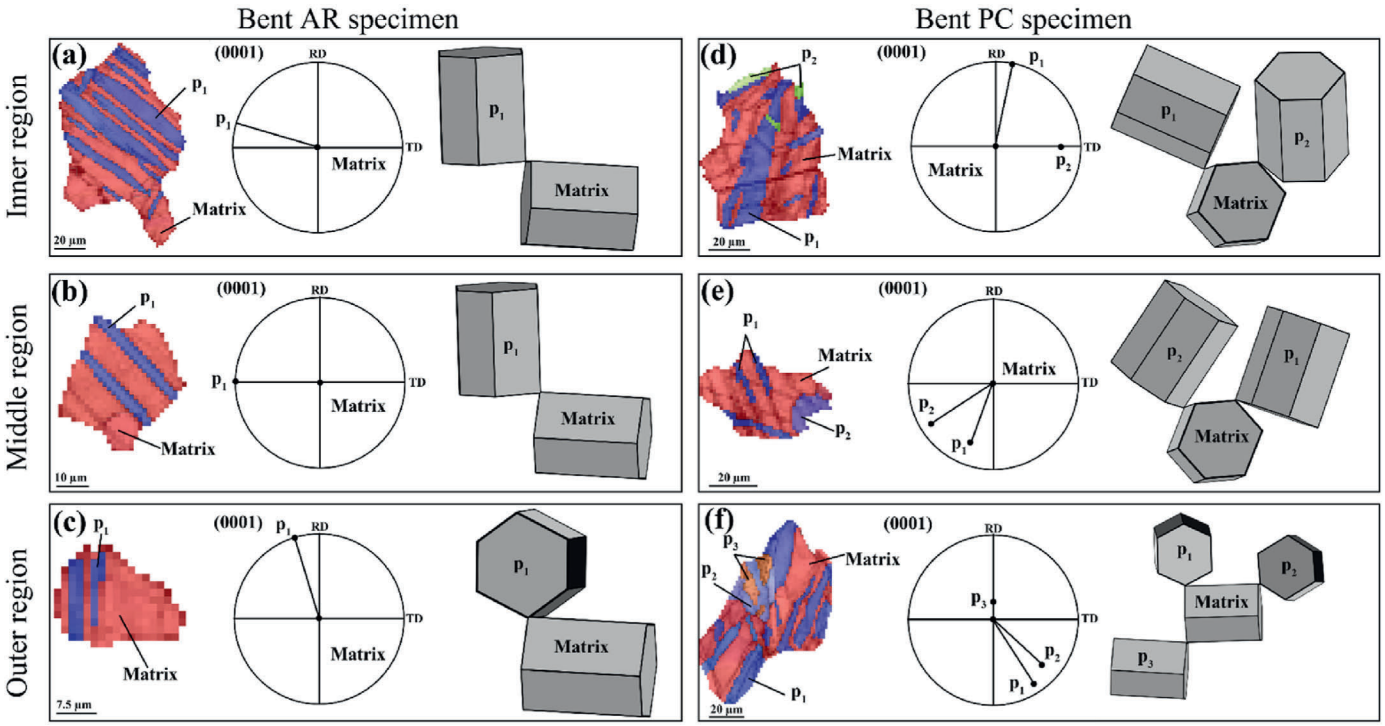

Fig. 6. Local twinning characteristics selected in different regions in Fig. 5: (a) (b) (c) bent AR specimen, and (d) (e) (f) bent PC specimen.

the twin orientation deviates from the center by approximately 90°, and the *c*-axis of the twin is nearly perpendicular to the *c*-axis of the matrix parent grain, further confirming that these twins are {10 $\bar{1}$ 2} tensile twins. In different regions of the bent AR specimen, the twin lamellae within the grains tend to be distributed in parallel. In contrast, the twinning in the bent PC specimen is relatively complex, with obvious intersecting twinning phenomena observed in different regions, which confirms that, in addition to pre-existing twins, new twins appeared during the bending process. Compared to the simple parallel twins within the grains of the bent AR specimen, the appearance of intersecting twins in the bent PC specimen further subdivides and refines the grains, which can significantly enhance the ability to coordinate strain within and between grains [17,31–33].

Fig. 7 displays the (0001) and (10 $\bar{1}$ 0) pole figures in different regions of the bent AR and PC specimens. For the bent AR specimen, the (0001) basal pole density shows a gradually increasing trend from the inner region to the outer region. This difference primarily stems from the varying degree of {10$\bar{1}$ 2} tensile twinning activation in each region. The compressive stress on the inner region of the bent AR specimen promotes {10$\bar{1}$ 2} twinning, which changes the grain orientation in the twinned regions, thus reducing the basal texture intensity from 17.47 in the AR specimen to 14.90. The deformation in the middle region of the bent AR specimen is relatively small, so the basal texture change is not obvious. The tensile stress on the outer region of the bent AR specimen is unfavorable for {10$\bar{1}$ 2} twinning and basal slip dominate the deformation, which enhances the basal texture intensity.

For the bent PC specimen, compared to the PC sample, the basal texture intensity in the inner and outer regions is enhanced. This may be attributed to the pre-existing twins promoting the rotation of the c-axis of the grain and an increased degree of basal slip, thereby enhancing the basal texture intensity. The deformation in the middle region of the bent PC specimen is also relatively small, so the texture change is not significant. It is worth noting that compared to the bent AR sample, the difference in basal texture intensity between the inner and outer regions of the bent PC specimen is smaller. This means that the deformation distribution is more uniform across the inner and outer regions of the bent specimen, which improves the material's tension-compression asymmetry, thus effectively reducing the cracking risk due to deformation incompatibility between the inner and outer regions of the bent specimen [34,35].

4. Discussion

As shown in Fig. 5, the degree of twinning in the inner region of the bent AR specimen is much higher than that in the outer region. This reflects the significant difference in tension-compression deformation capacity of the initial material with strong basal texture during the bending deformation process. For the PC specimen, the pre-existing twins changed the crystal orientation of part of the grains, reduced the basal texture intensity, and adjusted the material's response to subsequent tensile and compressive loads [22]. Compared to the AR specimen, the tension-compression asymmetry coefficient of the PC specimen is significantly improved (0.57 vs 0.35). The improvement in the tension-compression asymmetry leads to a more uniform strain distribution in different regions of the specimen during the bending process, avoiding excessive strain concentration in the tensile stress region or the compressive stress region. Furthermore, the pre-existing twins in the outer region of the bending sample may undergo detwinning when subjected to tension. This detwinning process itself can accommodate a part of the tensile strain and can activate other deformation modes [23,35].

As shown in Fig. 1, the AR specimen shows a strong basal texture. For the PC sample, as shown in Fig. 2, the pre-existing {10 $\bar{1}$ 2} twins lead to grain rotation by 86.3° towards the loading stress direction, thus forming a TD-oriented twin texture. Fig. 8 shows the Schmid factor maps for basal slip of the AR and PC specimens and a schematic diagram of basal slip during the bending deformation process. The Schmid factor for basal slip was calculated under the assumption of a uniaxial tensile stress state along the RD, which represents the dominant stress component in the outer region of the bent specimen, where tensile failure typically initiates. From Fig. 8a and b, it can be seen that compared to the AR specimen, the average Schmid factor for basal slip in the PC specimen increases from 0.19 to 0.26, which means basal slip is easier to activate

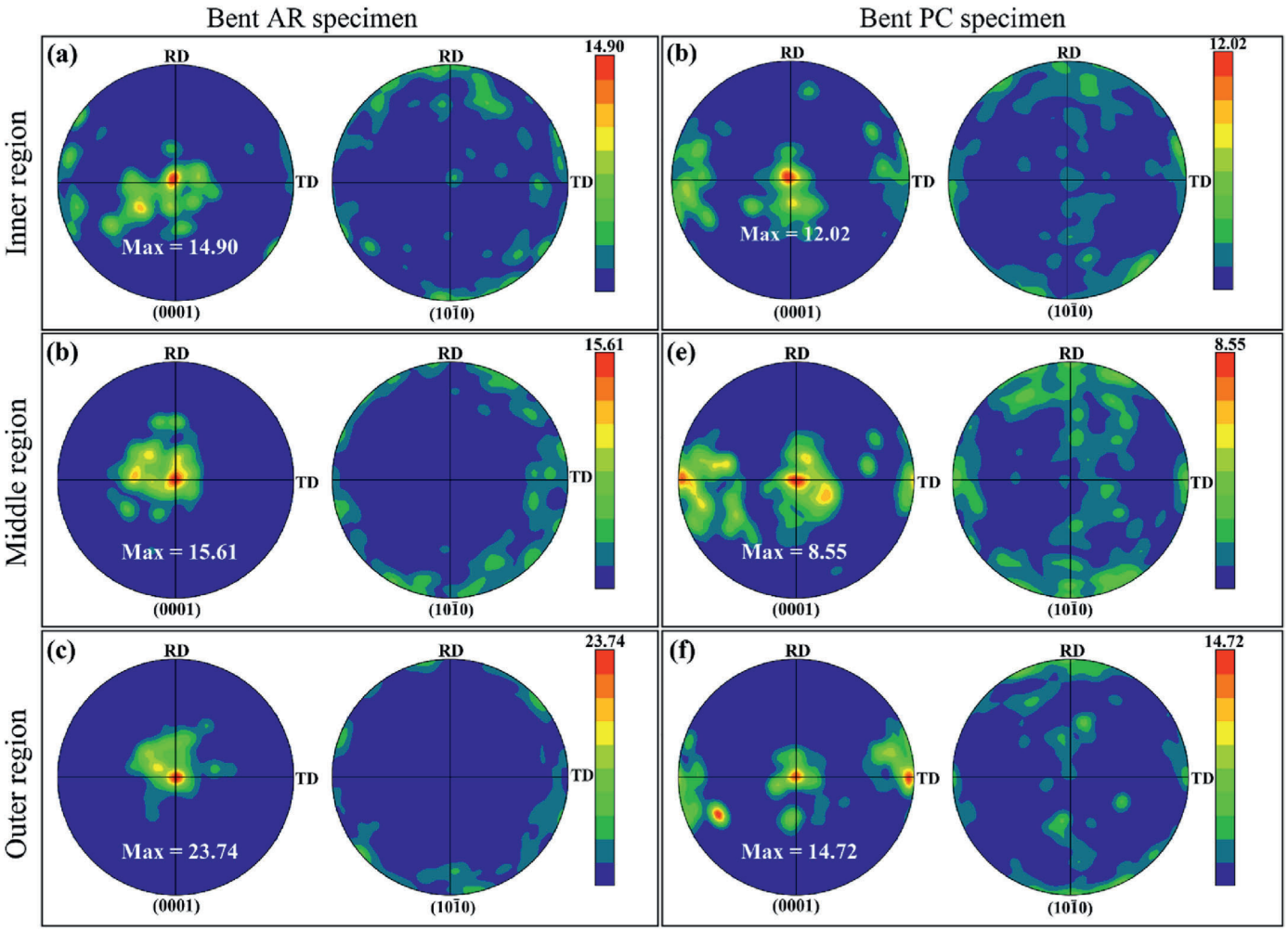

Fig. 7. (0001) and (10 $\bar{1}$ 0) poles in different regions of bent specimens: (a) (b) (c) bent AR specimen, and (d) (e) (f) bent PC specimen.

in the PC specimen [13]. Increased activation of basal slip contributes to increasing the bending fracture strain of Mg alloy. As can be seen from Fig. 8c, for the AR specimen with a stronger basal texture, its basal planes are mainly parallel to the RD-TD plane. During the bending deformation process, basal slip is difficult to accommodate strain along the *c*-axis direction of the grain and mainly contributes to strain along TD and RD. Therefore, for the AR specimen during bending, the thickness strain along ND can only be induced by {10 $\bar{1}$ 2} twinning or <c+a> slip [36–38]. However, since twinning can only produce very small strain [39], and the CRSS for <c+a> slip is relatively high at room temperature and difficult to activate, it is difficult for the AR specimen to produce the thick-direction strain during bending to coordinate the deformation, which is extremely unfavorable for its formability. As shown in Fig. 8d, for the PC specimen with a TD-oriented texture, the basal plane of some grains is parallel to the RD-ND plane. For the PC specimen during the bending deformation process, the activation of these basal slip systems is beneficial for the thickness strain along ND, which can improve the thickness deformation capacity of the Mg alloy plate, which is of important significance for the improvement of formability.

As shown in Figs. 1 and 2, compared to the AR specimen, the PC specimen has a smaller grain size (33.57 μm vs. 26.40 μm). Moreover, after bending deformation, the bent PC specimen also exhibits a smaller grain size in different regions of the bent sample (23.06 μm vs. 37.74 μm, 20.62 μm vs. 25.87 μm, 28.26 μm vs. 32.98 μm), as shown in Fig. 5. This can be attributed to the high-density layered twin boundaries introduced by pre-existing twins effectively refining the grains [16], which is of important significance for deformation coordination during the deformation process. As shown in Fig. 9, twin boundaries, acting as effective barriers to dislocation motion, subdivide the original grains into smaller structures, forming a "twinning-induced grain refinement" effect [16]. Furthermore, during the bending deformation process, for the PC specimen, new twins intersect with pre-existing twins, thereby subdividing and refining the grains more effectively. This reduction in effective grain size and the increase of internal interfaces improve the material's ability to coordinate intergranular strain incompatibility, promoting the uniform distribution of plastic deformation throughout the entire material. During the bending deformation process, more coordinated plastic deformation can reduce local stress concentration and strain gradient, thus retarding the initiation and propagation of microcracks.

In summary, the improvement in the bending formability of AZ31 Mg alloy can be attributed to the effect of pre-existing {10 $\bar{1}$ 2} twins. On the one hand, pre-existing {10$\bar{1}$ 2} twins lead to the rotation of the *c*-axis of the grain, altering the basal texture, which effectively improves the tension-compression asymmetry. The activation of basal slip on the RD-ND plane improves the thickness strain of the specimen during the bending deformation process. On the other hand, a large number of twin lamellae are introduced to effectively subdivide and refine the grains, thereby enhancing the uniform deformation capability and plastic deformation capability of the AZ31 Mg alloy during the bending deformation process.

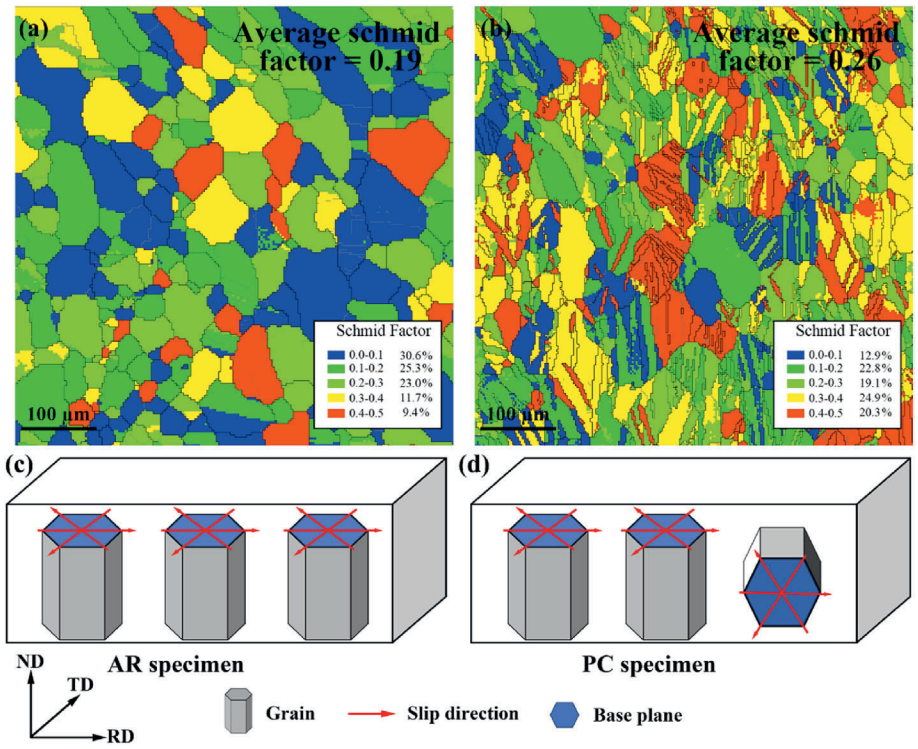

Fig. 8. Schmid factor maps and schematic diagrams for basal slip: (a) (b)AR specimen, and (c) (d) PC specimen.

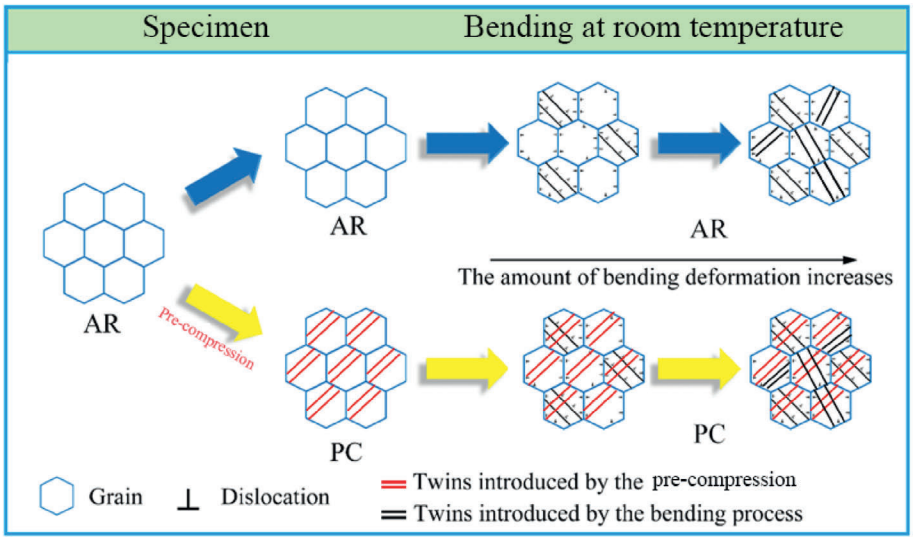

Fig. 9. Schematic diagrams of microstructure changes during the bending deformation process.

5. Conclusion

Pre-compression along TD was conducted on the hot-rolled AZ31 Mg alloy plate to introduce a large number of {10 $\bar{1}$ 2} tensile twins, aiming to improve its bending formability. The main conclusions are as follows:

(1) Compared to the AR specimen, the PC specimen with pre-existing {10 $\bar{1}$ 2} twins show higher tension yield strength (191 MPa vs. 151 MPa), compression yield strength (108 MPa vs. 53 MPa). The tension peak stress (305 MPa vs. 283 MPa), compression peak stress (302 MPa vs. 275 MPa), elongation (15.7 % vs. 12.8 %), and compression ratio (17.0 % vs. 15.1 %) also show corresponding increases.

(2) Pre-existing {10 $\bar{1}$ 2} tensile twins significantly improved the tension-compression yield asymmetry and bending formability of AZ31 Mg alloy. The tension-compression yield asymmetry coefficient increased from 0.35 to 0.57. Compared to the AR sample's bending angle of 65° and bending displacement of 7.3 mm, the PC sample achieved a bending angle of 97° and a bending displacement of 12.2 mm.

(3) Pre-existing {10 $\bar{1}$ 2} twins led to the rotation of the *c*-axis of the grain, altering the basal texture, effectively improving the tension-compression asymmetry, and activating the basal slip on the RD-ND plane that contributes to the thickness strain during bending. The introduction of a large number of twin lamellae effectively subdivided and refined the grains, thereby enhancing

the plastic deformation capability of AZ31 Mg alloy during bending. These factors ultimately led to a significant improvement in the bending formability of AZ31 Mg alloy.

CRediT authorship contribution statement

Longhui Sun: Writing – original draft, Validation, Investigation, Formal analysis. **Hongchen Jing:** Validation, Investigation. **Hua Zhang:** Writing – review & editing, Visualization, Resources, Methodology, Supervision. **Liying Sun:** Data curation, Conceptualization. **Lifei Wang:** Writing – review & editing. **Liwei Lu:** Writing – review & editing. **Kwang Seon Shin:** Writing – review & editing. **T.B. Duishenaliev:** Writing – review & editing.

Data availability

All data included in this study are available upon request by contacting the corresponding author.

Declaration of competing interest

The authors declare that they have no known competing financial interests or personal relationships that could have appeared to influence the work reported in this paper.

Acknowledgement

This study was supported by the National Natural Science Foundation of China (52274397), the Shandong Provincial Natural Science Foundation of China (ZR2024JQ020), and the Graduate Innovation Foundation of Yantai University, China (KGIFYTU2520).

References

[1] Y. Yuan, X. Chen, X.M. Xiong, K. Li, J. Tan, Y. Yang, X.D. Peng, X.H. Chen, D. L. Chen, F.S. Pan, Research advances of magnesium and magnesium alloys globally in 2024, J. Magnesium Alloys 13 (2025) 4689–4732.
[2] Y. Zheng, Y. Lu, H. Tong, J. Lu, D.L. He, Z.Y. Zhang, Y. Li, A novel hydrophilic-to-hydrophobic convertible coating on biodegradable Mg-4Zn-1Mn alloy: preparation, microstructure and corrosion behaviour, Prog. Nat. Sci. Mater. Int. 35 (2025) 752–763.
[3] T. Zhang, S. Wang, J. He, S.L. Wang, B. Yan, M.Q. Gong, W. Han, X.Y. Jiang, C. Shi, J. Xiang, In vitro and in vivo evaluation of high-strength Mg-Zn-Zr-Mn alloy: promising biocompatibility and degradation for medical translations, Prog. Nat. Sci. Mater. Int. 35 (2025) 339–350.
[4] J.Y. Zhang, F. Li, F.W. Kang, Z.Y. Wang, L. Sun, Double effects of recrystallization behavior on grain morphology evolution and mechanical properties of Al/Mg/Al composite plate by hard plate rolling, Prog. Nat. Sci. Mater. Int. 34 (5) (2024) 1029–1038.
[5] K. Zhang, Z.T. Shao, C.S. Daniel, M. Turski, C. Pruncu, L.L. Lang, J. Robson, J. Jiang, A comparative study of plastic deformation mechanisms in room-temperature and cryogenically deformed magnesium alloy AZ31, Mater. Sci. Eng. A 807 (2021) 140821.
[6] L. Zhang, Y. Li, Dynamic recrystallization mechanism, texture evolution development and mechanical characteristics of a Mg-8.7Gd-4.18Y-0.42Zr magnesium alloy by ECAP, Prog. Nat. Sci. Mater. Int. 34 (2) (2024) 376–388.
[7] U.M. Chaudry, H.M.R. Tariq, M. Zubair, N. Ansari, T.S. Jun, Implications of twinning on the microstructure development, crystallographic texture and mechanical performance of Mg alloys- a critical review, J. Magnesium Alloys 11 (2023) 4146–4165.
[8] J.U. Lee, S.H. Kim, Y.J. Kim, S.H. Park, Improvement in bending formability of rolled magnesium alloy through precompression and subsequent annealing, J. Alloys Compd. 787 (2019) 519–526.
[9] H.B. Chen, T.M. Liu, L.W. Lu, J.J. He, Y.B. Zhai, Influence of pre-strain and heat treatment on subsequent deformation behavior of extruded AZ31 Mg alloy, Trans. Nonferrous Met. Soc. China 25 (2015) 3604–3610.
[10] G.S. Huang, J.H. Li, T.Z. Han, H. Zhang, F.S. Pan, Improving low-cycle fatigue properties of rolled AZ31 magnesium alloy by pre-compression deformation, Mater. Des. 58 (2014) 439–444.
[11] H. Zhang, M.X. Yang, M.J. Hou, L.F. Wang, Q. Zhang, J.F. Fan, W.G. Li, H.B. Dong, S.M. Liu, B.S. Xu, Effect of pre-existing {10-12} extension twins on mechanical properties, microstructure evolution and dynamic recrystallization of AZ31 Mg alloy during uniaxial compression, Mater. Sci. Eng. A 744 (2019) 456–470.
[12] S.H. Park, S.-G. Hong, C.S. Lee, Enhanced stretch formability of rolled Mg-3Al-1Zn alloy at room temperature by initial {10-12} twins, Mater. Sci. Eng. A 578 (2013) 271–276.
[13] L. Jiang, J.J. Jonas, R.K. Mishra, A.A. Luo, A.K. Sachdev, S. Godet, Twinning and texture development in two Mg alloys subjected to loading along three different strain paths, Acta Mater. 55 (2007) 3899–3910.
[14] R.L. Shi, B. Song, D.B. Xia, T.T. Liu, Q.S. Yang, N. Guo, S.F. Guo, Influence of initial {10-12} twins on twinning behavior of extruded AZ31 alloys during free-end torsion, Mater. Char. 201 (2023) 112932.
[15] Y.P. Li, Y.J. Cui, H.K. Bian, S.H. Sun, N. Tang, Y. Chen, B. Liu, Y. Koizumi, A. Chiba, Detwining in Mg alloy with a high density of twin boundaries, Sci. Technol. Adv. Mater. 15 (2014) 35003.
[16] S. Wang, H.C. Pan, D.S. Xie, D.D. Zhang, J.R. Li, H.B. Xie, Y.P. Ren, G.W. Qin, Grain refinement and strength enhancement in mg wrought alloys: a review, J. Magnesium Alloys 11 (2023) 4128–4145.
[17] Y.B. Hu, M.S. Guan, T.X. Zheng, Microstructure, mechanical properties and yield asymmetry of Mg-4A1-2Sn-xY alloys, Mater. Sci. Technol. 34 (9) (2018) 1131–1141.
[18] X.H. Zhang, J.Q. Li, L. Wang, Y.S. Cheng, W. Lei, Q. Chen, <c + a> slip-dominated deformation mechanisms and tensile anisotropy of rolled Mg-6.3Gd-3Li-2Zn-0.5Al alloy based on crystal plasticity analysis, J. Magnesium Alloys 13 (10) (2025) 5243–5262.
[19] M. Arul Kumar, I.J. Beyerlein, C.N. Tomé, A measure of plastic anisotropy for hexagonal close packed metals: application to alloying effects on the formability of Mg, J. Alloys Compd. 695 (2017) 1488–1497.
[20] S. Jayasathyakawin, M. Ravichandran, N. Baskar, C. Anand Chairman, R. Balasundaram, Mechanical properties and applications of magnesium alloy - review, Mater. Today Proc. 27 (2) (2020) 909–913.
[21] Y.J. Wang, Y. Zhang, H.T. Jiang, Tension compression asymmetry and corresponding deformation mechanism in ZA21 magnesium bars with bimodal structure, Int. J. Miner. Metall. Mater. 30 (2023) 92–103.
[22] J.B. Go, M.H. Park, S. Gao, H. Matsumiya, W. Gong, N. Tsuji, Loading-direction dependence of non-basal slip activity in a pre-twinned AZ31 magnesium alloy, J. Alloys Compd. 1014 (2025) 178749.
[23] Y.X. You, L. Tan, Y.Q. Yan, T. Zhou, P.F. Yang, J. Tu, Z.M. Zhou, Towards understanding {10-11}-{10-12} secondary twinning behaviors in AZ31 magnesium alloy during fatigue deformation, Materials 17 (2024) 1594.
[24] X. Zeng, S.B. Yi, Deformation mechanisms of magnesium alloys with rare-earth and zinc additions under plane strain compression, Materials 17 (2023) 33.
[25] Z. McClelland, B. Li, S.J. Horstemeyer, S. Brauer, A.A. Adedoyin, L.G. Hector, M. F. Horstemeyer, Geometrically necessary twins in bending of a magnesium alloy, Mater. Sci. Eng. A 645 (2015) 298–305.
[26] M.R. Barnett, Twinning and the ductility of magnesium alloys: part II. "Contraction" twins, Mater. Sci. Eng. A 464 (2007) 8–16.
[27] K.D. Molodov, T. Al-Samman, D.A. Molodov, Profuse slip transmission across twin boundaries in magnesium, Acta Mater. 124 (2017) 397–409.
[28] D. Drozdenko, J. Bohlen, S. Yi, P. Minárik, F. Chmelík, P. Dobroň, Investigating a twinning-detwinning process in wrought Mg alloys by the acoustic emission technique, Acta Mater. 110 (2016) 103–113.
[29] L.F. Wang, G.S. Huang, Q. Quan, P. Bassani, E. Mostaed, M. Vedani, F.S. Pan, The effect of twinning and detwinning on the mechanical property of AZ31 extruded magnesium alloy during strain-path changes, Mater. Des. 63 (2014) 177–184.
[30] J.X. Wang, M.A. Kumar, I.J. Beyerlein, Investigation of crossed-twin structure formation in magnesium and magnesium alloys, J. Alloys Compd. 935 (2023) 168094.
[31] Y. Yue, J. Wang, J.F. Nie, Twin-solute, twin-dislocation and twin-twin interactions in magnesium, J. Magnesium Alloys 11 (2023) 3855–3887.
[32] Q. Yu, J. Wang, Y.Y. Jiang, R.J. McCabe, N. Li, C.N. Tomé, Twin-twin interactions in magnesium, Acta Mater. 77 (2014) 28–42.
[33] W.Z. Chen, W.J. Wu, W.K. Wang, W.C. Zhang, X.H. Liu, H.S. Kim, Adjusting approaches of basal texture for improvement of tension-compression asymmetry in extruded magnesium alloys, Mater. Res. Lett. 11 (2023) 563–570.
[34] S. Kurukuri, M.J. Worswick, D. Ghaffari Tari, R.K. Mishra, J.T. Carter, Rate sensitivity and tension-compression asymmetry in AZ31B magnesium alloy sheet, Philos. Trans. R. Soc. Math. Phys. Eng. Sci. 372 (2014) 20130216.
[35] T. Hama, N. Kitamura, H. Takuda, Effect of twinning and detwinning on inelastic behavior during unloading in a magnesium alloy sheet, Mater. Sci. Eng. A 583 (2013) 232–241.
[36] J.U. Lee, Y.J. Kim, S.-H. Kim, J.H. Lee, M.S. Kim, S.H. Choi, B.G. Moon, Y.M. Kim, S.H. Park, Texture tailoring and bendability improvement of rolled AZ31 alloy using {10-12} twinning: The effect of precompression levels, J. Magnes. Alloys 7 (2019) 648–660.
[37] S.R. Agnew, Ö. Duygulu, Plastic anisotropy and the role of non-basal slip in magnesium alloy AZ31B, Int. J. Plast. 21 (2005) 1161–1193.
[38] Y.B. Pei, E.B. Wei, M.J. Yao, M.H. Yu, M.S. Zhao, B.G. Teng, Plastic deformation mechanism of Mg-Gd-Y-(Sm)-Zr alloys at room and cryogenic temperature, Rare Met. 44 (2025) 2778–2790.
[39] Y. Chino, K. Kimura, M. Mabuchi, Deformation characteristics at room temperature under biaxial tensile stress in textured AZ31 Mg alloy sheets, Acta Mater 57 (2009) 1476–1485.